23

SIMULATION OF SEMICONDUCTOR DEVICES AND PROCESSES Vol. 4
Edited by W. Fichtner, D. Aemmer - Zurich (Switzerland) September 12-14, 1991 - Hartung-Gorre

Physical Modelling for Bipolar Device Simulation

D.B.M. Klaassen

Philips Research Laboratories, 5600 JA Eindhoven, The Netherlands

Abstract

Recent developments in physical models for device simulation are discussed. The discussion focusses on the incorporation of tunnelling effects in the generation-recombination of charge carriers, on the unified modelling of the majority and minority carrier mobility and on a resulting model for the bandgap narrowing valid for both n- and p-type silicon.

1 Introduction

For device simulation four basic physical phenomena have to be modelled:

- generation and recombination of charge carriers;
- charge carrier mobility;
- intrinsic carrier concentration and bandgap narrowing; and
- boundary conditions at interfaces and contacts.

The results of device simulations depend critically on the accuracy of the models for these physical phenomena. Modern trends in IC technology are towards lateral downscaling and shallow emitter and base profiles. At the same time dopant concentrations are increased in order to maintain proper electrical characteristics of the bipolar transistors (e.g. prevent punch-through). These increased dopant concentrations lead to high electrical fields around the p-n junctions. Both high dopant concentrations and high electrical fields evoke new physical mechanisms. The non-ideal base current increases and shows an anomalous temperature behaviour (see [1 – 5] and Fig. 3), whereas the leakage current under reverse-bias also increases (see e.g. [5] and Fig. 4). Moreover, on special test structures the minority carrier mobility is shown to exceed the majority carrier mobility at high dopant concentrations by a factor of about three (see [6 – 10] and Figs. 7 and 8). At high dopant concentrations the p-n product increases, which is modelled through the apparent bandgap narrowing. The literature seems to suggest that this apparent bandgap narrowing is different in n-type and p-type silicon (see [6, 7, 11 – 13] and Fig. 17).

All effects mentioned above will have to be modelled in order to ensure accurate device simulations. In this paper we will concentrate on models for drift-diffusion simulators, these being the workhorse for most device physicists and engineers. Models for generation and/or recombination including the effects of high electrical fields, for carrier mobility and for bandgap narrowing will be discussed in the next sections. Models for the physical mechanisms at interfaces and contacts are not discussed, firstly, because they are not affected by high dopant concentrations and, secondly, because excellent reviews of the widely-used poly-silicon contacts are available [14, 15].

2 Generation and recombination

2.1 Introduction

Most textbooks distinguish three physical processes leading to the generation and/or recombination of charge carriers in silicon (see e.g. [16, 17]):

- Shockley-Read-Hall generation/recombination;
- Auger generation/recombination; and
- impact ionization or avalanche multiplication.

For devices in which a direct semiconductor, e.g. GaAs, is exposed to light also generation/recombination involving absorption/emission of photons may have to be considered.

The Shockley-Read-Hall generation/recombination describes the emission and capture, respectively, of electrons and holes by defects or traps with energy levels in the forbidden zone [18] . As this type of recombination/generation is especially effective in the depleted regions at the junctions, it is likely to be affected by the increased electrical fields around these junctions. These effects will be discussed in Subsects. 2.2 - 2.4.

The Auger recombination/generation is a three-particle process: an electron and a hole recombine, transferring the excess energy to a third carrier, or an electron and a hole are generated, consuming the excess energy of a third carrier (see e.g. [19, 20] and references cited therein). This type of recombination prevails in highly-doped neutral regions. At increased dopant levels Auger recombination/generation becomes even more important. No experimental evidence has been published indicating that the existing description is inadequate. Therefore it is not discussed here.

Impact ionization occurs when electrons (and/or holes) gain so much energy in a high electrical field, that they can excite electrons from the valence into the conduction band. The electron-hole pair thus created may in its turn take part in the process, creating an avalanche multiplication (see e.g. [21 – 23]). This generation process occurs in the depletion regions under high reverse-bias. Increasing dopant concentrations and the resulting elevated electrical fields will lead to avalanche breakdown at lower reverse-bias voltages. In drift-diffusion simulators the ionization coefficients are modelled as functions of the electrical field. In simulators solving the hydrodynamic device equations these ionization coefficients are modelled as a function of carrier temperature, which may be expected to yield more realistic results. For the normal bipolar DC characteristics drift-diffusion simulators mostly suffice.

At intermediate dopant concentrations the lifetime of the carriers in *bulk* silicon is determined by the *conventional* Shockley-Read-Hall generation/recombination and at high dopant concentrations by Auger generation/recombination. Only very limited experimental data have been published on the temperature dependence of the carrier lifetime [20, 24] . As the latter is important in the interpretation of minority carrier diffusion length measurements as a function of temperature, this dependence will be discussed in Subsect. 3.9.

2.2 Trap-assisted tunnelling under forward-bias

At high electrical fields in narrow depletion regions charge carriers are no longer restricted to the valence and conduction band, but can tunnel into the forbidden zone (see Fig. 1). This tunnelling process leads to an enlarged electron concentration, n_t, in the depletion region [4, 5]

$$n_t(x) = n(x) + Ai^{-2}(0) \int_0^x \left(-\frac{dn(x)}{dx} \right)_{x = x_1} Ai^2(y[x - x_1]) \, dx_1 , \qquad (1)$$

and a similar expression for the enlarged hole concentration p_t. The first term on the right-hand side of Eq. (1) is the conventional injected electron density and the second term on the right-hand side is the tunneling contribution. Herein Ai is the Airy function; $y = (2q\overline{F}m^* \hbar^{-2})^{1/3}$; $\overline{F}$ is the average electrical field and m^* is the tunnelling effective mass. The physical meaning of $Ai^2(y[x - x_1])$ is the probability that an electron at x_1 will tunnel to a trap at x (see Fig. 1). In the case where the trap depth $(E_c - E_t)$ is less than $q\overline{F}x$, the lower bound in the integral must be replaced by $x - (E_c - E_t)/q\overline{F}$.

Due to these enlarged electron and hole concentrations the recombination current under forward-bias will increase. This phenomenon is usually referred to as forward-biased tunnelling or the excess current.
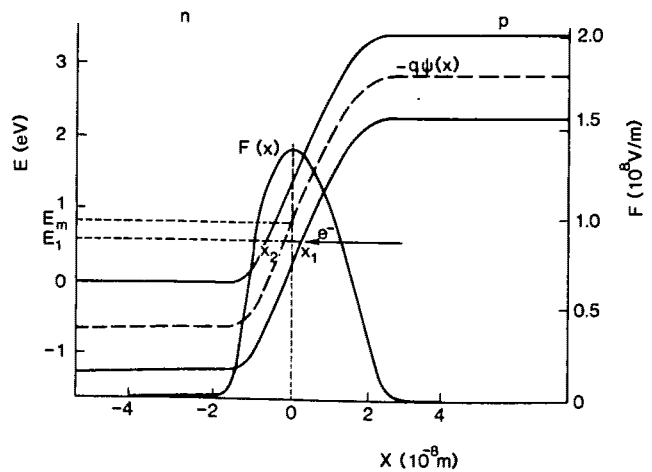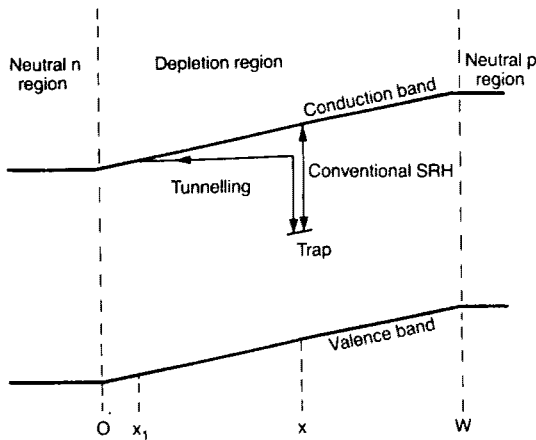
Figure 1 (left-hand side): Schematic energy-band diagram of a forward-biased pn junction. Both the conventional SRH process and the trap-assisted tunnelling process are denoted (figure taken from [5]).

Figure 2 (right-hand side): An example of the actual electric field and potential energy around a p-n junction. $x = 0$ is at the electrical junction (figure taken from [26]).

2.3 Trap-assisted tunnelling under reverse-bias

The emission of electrons and holes from traps is also affected by tunnelling, because the multiphonon transition takes place over only part of the trap depth. Following Vincent et al. [25] the ratio of the emission probabilities with and without electric field is [5]

$$r_n = 1 + Ai^{-2}(0) \int_0^{\frac{(E_c - E_t)}{kT}} e^z Ai^2 \left(\frac{2m^* kT}{\gamma^2 \hbar^2} z \right) dz , \tag{2}$$

with a similar expression holding for r_p. In the integrand the Airy function is again the tunnelling probability, whereas the Boltzmann factor describes the multiphonon transition probability. Near the edge of the depletion region the upper bound must be replaced by $q\bar{F}x/kT$.

Due to the enhanced emission probabilities for electrons and holes the generation current under reverse-bias will increase.

2.4 Band-to-band tunnelling

With increasing electrical fields the contribution of the multiphonon transition to the emission probability given by Eq. (2) decreases and the tunneling contribution increases. Finally direct band-to-band tunnelling becomes important (from x_1 to x_2 in Fig. 2). An expression for the generation due to this process is obtained by a transformation of Kane's expression [27] for the current density per unit energy dJ_t/dE into a local generation rate, R_t, (see [5])

$$R_t = \frac{-1}{q} \underline{\nabla} \cdot \underline{J_t} = \frac{-1}{q} \frac{dJ_t}{d\psi} \cdot \underline{\nabla}\psi = -\frac{dJ_t}{dE} \cdot \underline{E} , \tag{3}$$

where $\underline{E}$ is the local electrical field [26] .

2.5 Model evaluation

The enlarged carrier concentrations and the enhanced emission probabilities described above can be incorporated in the Shockley-Read-Hall formulation. Adding the generation rate due to band-to-band tunnelling, the three tunnelling mechanisms described above yield the following expression for the recombination rate [5]

$$R = \frac{n_t p_t - r_n r_p n_i^2}{\tau_p(n_t + r_n n_i) + \tau_n(p_t + r_p n_i)} - B F^{5/2} e^{-F_0/F} , \tag{4}$$

where the last term on the right-hand side, describing the generation due to band-to-band tunnelling, should be taken into account only in reverse bias. Furthermore it should be noted that F_0 has the same temperature dependence as the bandgap [26] . Evaluation of the ex-

pression given by Eq. (4) is greatly facilitated by the fact that $n_i(x)/n(x) \simeq r_n$ (and similarly for holes). Moreover, for the integral in the expression for r_n given by Eq. (2), analytical approximations can be found. For low values of the electrical field the expression given by Eq. (4) reduces to the conventional Shockley-Read-Hall expression. Consequently, terms describing the Auger generation/recombination and impact ionization should be added to the expression given by Eq. (4). Using this model good agreement between measurements and calculations on non-ideal base currents as well as on leakage currents under reverse-bias has been obtained, as can be seen from Figs. 3 and 4 (NEW; see [5]).

In these figures also results obtained with the models of del Alamo and Swanson (DAS; see [1, 2]) and of Woo et al. (WPS; see [3]) are shown. Del Alamo and Swanson give a semi-emperical expression for the tunnelling current density under forward-bias. Even after re-fitting of the parameters involved the temperature dependence was too weak (DAS-FIT; see Fig. 3 and [5]). This is caused by the fact that only tunnelling from $x_1 = 0$ to $x_1 = W$ is taken into account (see Fig. 1) and multiphonon transitions are neglected. Moreover, an expression for the current density is less suited for device simulation.

Woo et al. give an expression for the enhanced recombination under forward-bias. They take only barrier lowering into account (Poole-Frenkel effect) and neglect tunnelling effects. Consequently their model (WPS) predicts, like the conventional Shockley-Read-Hall model (SRH), too strong a temperature dependence.

Finally, recently Voldman et al. presented an extension of the generation term in the model of Hurkx et al. [28]. Voldman et al. take barrier lowering and 3-D tunneling effects explicitly into account and arrive at very complicated expressions, that can only be used for
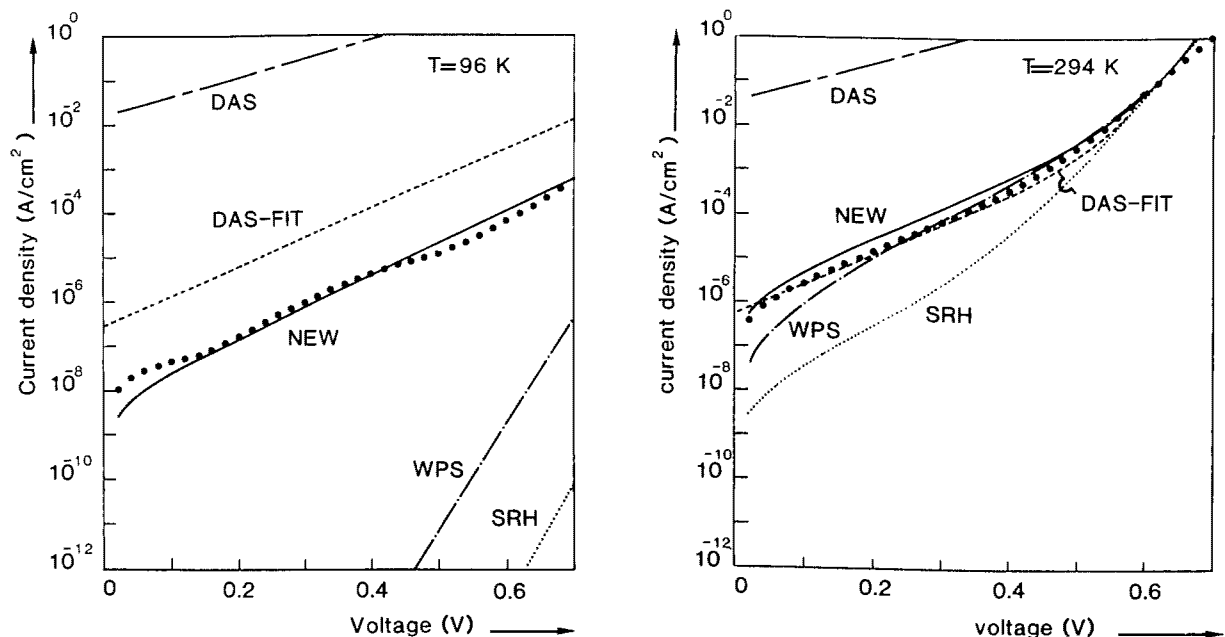
Figure 3: Measured I-V characteristics (dots) and predictions from various models (lines) for a diode at T = 96K (left-hand side) and T = 294K (right-hand side) respectively (figure taken from [5]).
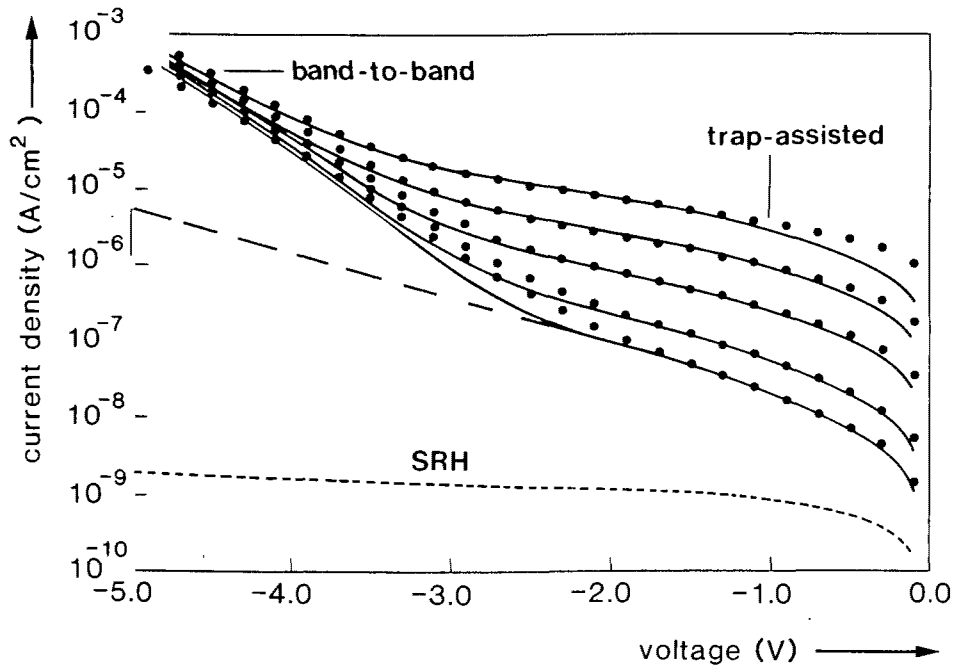
Figure 4: Measured (dots) and calculated (lines) reverse characteristics at different temperatures (starting from top T = 392, 365, 338, 311 and 295K). The dotted lines denotes the conventional SRH model and the dashed line is the trap-assisted tunnelling contribution, both at T = 295K (figure taken from [5]).

the description of reverse characteristics. Moreover, it should be noted that the effects of Coulomb interaction including barrier lowering, can effectively be described in the model of Hurkx et al. by a minor change in m^* [5] .

3 Charge carrier mobility

3.1 Introduction

For device simulation purposes the charge carrier mobility is mostly modelled as a function of total impurity concentration and no distinction between majority carriers and minority carriers is made. Several analytical fit functions have been suggested to describe the minority electron mobility (see [6] and Fig. 7) and minority hole mobility (see [7 – 9] and Fig. 8). Straightforward use of these functions implies that at each point in the device structure it should be decided whether a charge carrier is a minority or a majority carrier. This may lead to discontinuities in the mobility around the junctions. In order to prevent these discontinuities, the carrier mobility should be expressed as a *single* function of donor and acceptor concentrations. Moreover, electron-hole scattering has to be taken accurately into account because for the minority carrier mobility it is as important as impurity scattering.

Shigyo et al. [29] published a model for the carrier mobility combining the model for the majority carrier mobility of Masetti et al. [30] with the analytical fit functions for the minority carrier mobility mentioned above. However, electron-hole scattering was not taken into account and no temperature dependence was incorporated in the model.

Recently Klaassen [31] presented a model for the carrier mobility in which e.g. for electrons, both the electron-acceptor scattering mobility and the electron-hole scattering mobility were incorporated. Moreover, the different temperature dependence of majority and minority mobility was included in the model. This last model will be discussed in some detail in the next subsections. Only expressions for the electron mobility will be given. For holes similar expressions can be derived.

3.2 Lattice scattering

The electron mobility due to lattice scattering, $\mu_{e,L}$, is obtained from the low-concentration limit of the model of Masetti et al. [30] :

$$\mu = \mu_{min} + \frac{\mu_{max} - \mu_{min}}{1 + (N/N_{ref,1})^{\alpha_1}} - \frac{\mu_1}{1 + (N_{ref,2}/N)^{\alpha_2}} . \tag{5}$$

Including the temperature dependence this results in the following expression [31] :

$$\mu_{e,L} = \mu_{max} \left(\frac{300}{T} \right)^{\theta_e} . \tag{6}$$

The parameter θ_e has to be determined from a comparison with experimental data. The parameters in Eq. (5) for electrons and holes can be found in [30] .

3.3 Donor scattering including screening

The third term on the right-hand side of Eq. (5) is negligible up to doping levels of 10^{20} cm^{-3}. Effects of ultra-high concentrations on the carrier mobility will be discussed in Subsect. 3.6. The electron mobility due to donor scattering, $\mu_{e,D}$, is obtained by subtracting the lattice scattering mobility, $\mu_{e,L}$, from Eq. (5) using Matthiessen's rule. Screening of the impurities by charge carriers is taken into account by modifying the resulting expression for $\mu_{e,D}$ according to the the statistical screening theory of Ridley [32], which merges the Conwell-Weisskopf and Brooks-Herring approaches. The ultimate expression for $\mu_{e,D}$, including the temperature dependence, then reads [31]

$$\mu_{e,D}(N_D, c) = \mu_{e,N} \left(\frac{N_{ref,1}}{N_D} \right)^{\alpha_1} + \mu_{e,c} \left(\frac{c}{N_D} \right) , \tag{7a}$$

$$\text{with} \quad \mu_{e,N} = \frac{\mu_{max}^2}{\mu_{max} - \mu_{min}} \left(\frac{T}{300} \right)^{3\alpha_1 - 1.5} , \tag{7b}$$

and $\mu_{e,c} = \dfrac{\mu_{min}\,\mu_{max}}{\mu_{max} - \mu_{min}} \left(\dfrac{300}{T}\right)^{0.5}$, $\qquad\qquad$ (7c)

where c is the total carrier concentration. No additional parameters are introduced in Eqs. (7). It should be noted that electron-electron scattering is not accounted for, as it represents only a second order effect [32] .

3.4 Acceptor scattering

At low temperatures and high concentrations an attractive potential scatters charge carriers more effectively than a repulsive potential [33] . Because the Born approximation breaks down under these conditions, the partial-wave method was used to calculate the ratio, $G(P)$, between the collision cross-sections for repulsive $(\sigma_{\tau,rep})$ and attractive $(\sigma_{\tau,attr})$ screened Coulomb potentials

$$G(P) = \frac{\sigma_{\tau,rep}}{\sigma_{\tau,attr}} = \frac{\sigma_{min}}{\sigma_{maj}} = \frac{\mu_{maj}}{\mu_{min}} = \frac{\mu_{e,D}}{\mu_{e,A}} \ , \qquad\qquad (8)$$

as a function of $\quad P = 4\,k^2\,r_o^{\,2} \propto \dfrac{1}{c}$, $\qquad\qquad$ (9)

where k is the wave vector and r_o is the Debye screening length [32] (see Fig. 5). The contribution to the electron mobility due to acceptor scattering, $\mu_{e,A}$, is now obtained from
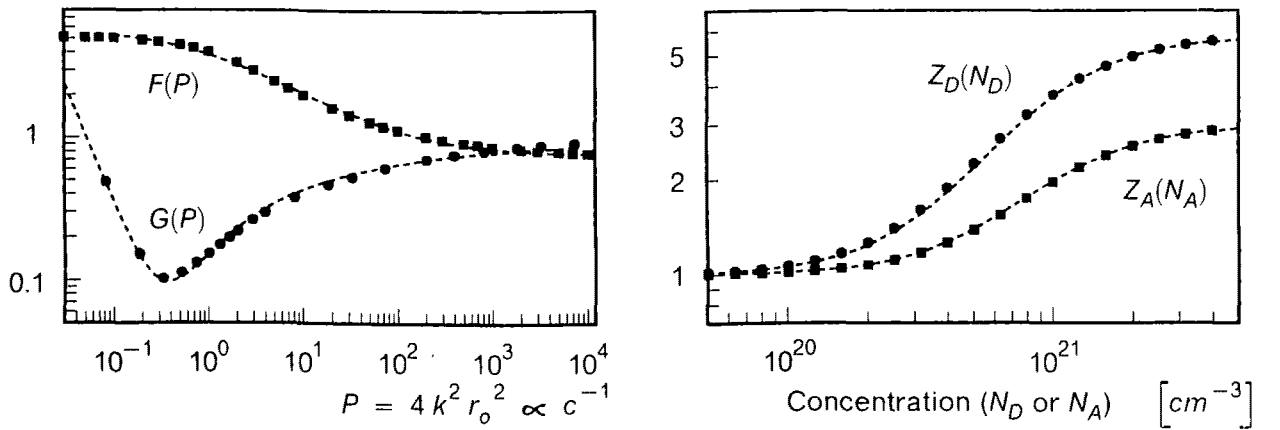
Figure 5 (left-hand side): The function $G(P) = \mu_{e,D} / \mu_{e,A}$ *for a temperature of 300K (solid circles) and the function* $F(P) = \mu_{e,h} / \mu_{e,D}$ *for a mass ratio equal to unity (solid squares). The dashed lines represent analytical fit functions describing the results of the calculations (figure taken from* [31] *).*

Figure 6 (right-hand side): *The clustering functions* Z_D *(solid circles) and* Z_A *(solid squares) as a function of* N_D *and* N_A *, respectively. The dashed lines represent analytical fit functions describing the results of the calculations (figure taken from* [31] *).*

$$\mu_{e,A}(N_A, c) = \frac{\mu_{e,D}(N_D = N_A, c)}{G(P)} \; . \tag{10}$$

3.5 Hole scattering

As far as the interaction potential is concerned, holes can be regarded as moving donors. The mobility ratio, $F(P)$, between stationary secondary scatterers with infinite mass and moving secondary scatterers with finite mass can be calculated accurately using the Born approximation (see Fig. 5), which yields for attractive potentials almost the same collision cross-sections as the partial-wave method. The contribution to the electron mobility due to hole scattering, $\mu_{e,h}$, is now obtained using

$$\mu_{e,h}(p, c) = F(P) \, \mu_{e,D}(N_D = p, c) \; , \tag{11}$$

where p is the hole concentration. It should be noted that as $F(P) \leq 1 / G(P)$, carrier scattering is more important for the minority carrier mobility than impurity scattering.

3.6 Ultra-high concentration effects

The effects of ultra-high concentrations on the mobility represented by the third term on the right-hand side of Eq. (5), can be accounted for by assuming that above an impurity concentration of 10^{20} cm^{-3} the carriers are no longer scattered by impurities possessing one electronic charge and a concentration N, but by impurities with Z electronic charges and a "cluster" concentration $N' = N/Z$. The concentration of charge carriers, c, is not affected. This implies that these ultra-high concentration effects on the carrier mobility can effectively be modelled by replacing N by $Z(N) N$, where $Z(N)$ is the "clustering" function (see Fig. 6 and [31]).

3.7 Model equations

In order to obtain the electron mobility, μ_e, as a function of N_D, N_A, n, p, and T one proceeds as follows.

Starting with ionized donor and acceptor concentrations, N_D and N_A, respectively, the clustering functions have to be applied to calculate the concentrations to be used in the model

$$N_D \to Z_D(N_D) \, N_D \quad \text{and} \quad N_A \to Z_A(N_A) \, N_A \; . \tag{12}$$

The problem of weak screening ($P \to \infty$ if $c \to 0$) is solved by taking for the parameter P a weighted harmonic mean of the expression given by Eq. (5) and its equivalent in the Conwell-Weisskopf approach (cf. the statistical screening theory of Ridley [32]) :

$$P_e = \left\{ \frac{n + p}{3.6 \times 10^{19}} + \left(\frac{N_{e,sc}}{6.5 \times 10^{19}} \right)^{2/3} \right\}^{-1} \left(\frac{T}{300} \right)^2 , \tag{13}$$

where $\quad N_{e,sc} = N_D + N_A + p$ (14)

is the sum of the concentrations of all scattering partners; all concentrations are in cm^{-3}.

Using Matthiessen's rule the electron mobility, μ_e, is now

$$\mu_e^{-1} = \mu_{e,L}^{-1} + \mu_{e,D}^{-1} + \mu_{e,A}^{-1} + \mu_{e,h}^{-1} \equiv \mu_{e,L}^{-1} + \mu_{e,D+A+h}^{-1} , \qquad (15)$$

where $\mu_{e,D+A+h}$ is given by the following expression [31]

$$\mu_{e,D+A+h}(N_D, N_A, n, p) = \mu_{e,N} \frac{N_{e,sc}}{N_{e,sc,eff}} \left(\frac{N_{ref,1}}{N_{e,sc}} \right)^{\alpha_1} + \mu_{e,c} \left(\frac{n+p}{N_{e,sc,eff}} \right) , \qquad (16)$$

$$\text{with} \quad N_{e,sc,eff} = N_D + G(P_e) N_A + \frac{p}{F(P_e)} . \qquad (17)$$

3.8 Model evaluation

3.8.1 Majority carrier mobility vs. impurity concentration

The model described above yields for the majority carrier mobility exactly the results of Eq. (5), which has been shown to be in good agreement with experimental data (see [30, 31]).
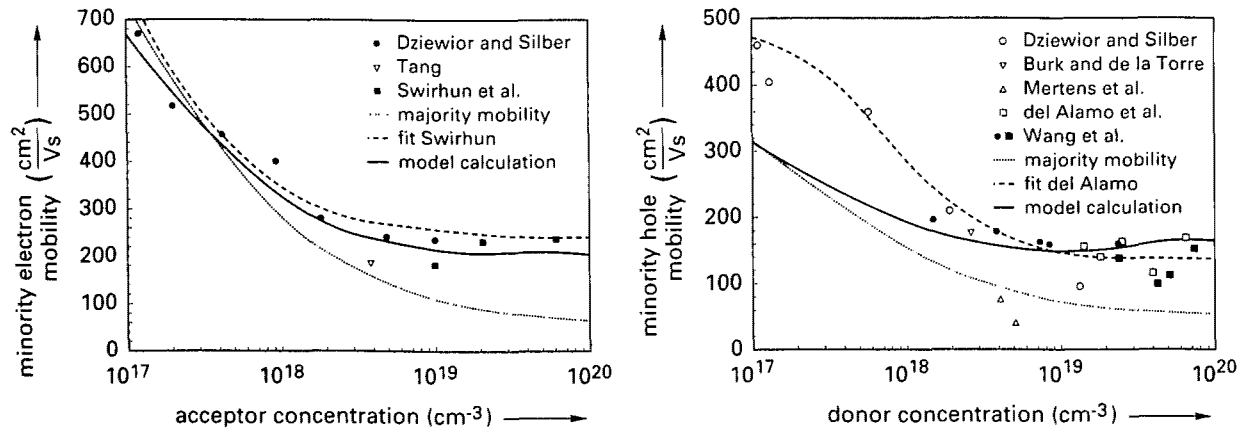
Figure 7 (left-hand side): Minority electron mobility as a function of acceptor concentration: symbols represent literature data [6, 34, 35] ; the dashed curve represents the fit of Swirhun et al. [6] ; the solid curve represents the new model [31] ; and the dotted curve represents the majority electron mobility.

Figure 8 (right-hand side): Minority hole mobility as a function of donor concentration: symbols represent literature data [7 – 10, 34, 36, 37] ; the dashed curve represents the fit of del Alamo et al. [7, 8] ; the solid curve represents the new model [31] ; and the dotted curve represents the majority electron mobility.

3.8.2 Minority carrier mobility vs. impurity concentration

In Figs. 7 and 8 the model calculations for the minority electron and hole mobility are compared with experimental data and analytical fit functions suggested in the literature. From these figures it can be seen that especially with the more recent data good agreement is obtained. However, at low concentrations the new model yields a minority hole mobility which is distinctly different from the experimental data [34] and the analytical fit function of del Alamo et al. [7, 8]. Both the experimental data and the fit show at a concentration of $10^{17} cm^{-3}$ no scattering for minority holes additional to the lattice scattering. However, in the next subsection it will be shown that electron-hole scattering is important at this concentration. Due to this electron-hole scattering and additional hole-donor scattering the new model yields a minority hole mobility that is substantially smaller than the lattice scattering mobility.

3.8.3 The effect of electron-hole scattering

Dannhäuser [38] and Krausse [39] measured the sum of electron and hole mobility in the intrinsic region of a pin-diode as a function of the injected carrier density ($n = p$; see Fig. 9). In the intrinsic region only lattice scattering and electron-hole scattering play a role. From Fig. 9 it can be seen that the new model describes the decrease in mobility due to electron-hole scattering quite well.

It should be noted that both this effect of electron-hole scattering and the temperature dependence (see next subsections) are not described by the model of Shigyo et al. [29] mentioned in the introduction.
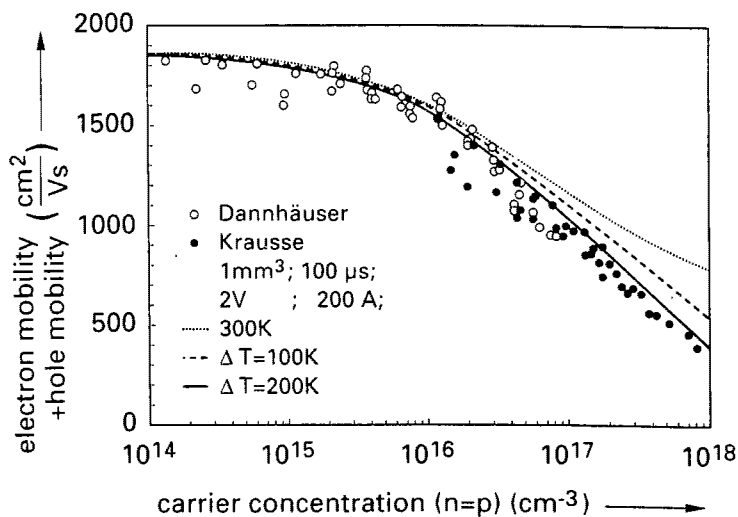
Figure 9: Sum of electron and hole mobility as a function of carrier concentration. Symbols represent experimental data measured in the intrinsic region of a pin-diode as function of the injected carrier density ($n = p$): open circles [38]; and solid circles [39]. Curves indicate model calculations without temperature increase (dotted curve) and with a temperature increasing linearly with carrier concentration from $300K$ at low concentrations to $400K$ (dashed curve) and $500K$ (solid curve) at $10^{18} cm^{-3}$.

3.8.4 Majority carrier mobility as a function of temperature

In Figs. 10 and 11 the majority carrier mobility is shown as a function of temperature for various dopant concentrations. A good agreement between experimental data and model calculations is obtained.

For the majority electron mobility only the lattice scattering and the electron-donor scattering are important. The expression for the electron-donor scattering mobility (Eq. (7)) contains no adjustable parameter. The value obtained for the parameter θ_e in the expression for the lattice scattering mobility is 2.29 (while for holes $\theta_h = 2.25$ was found).
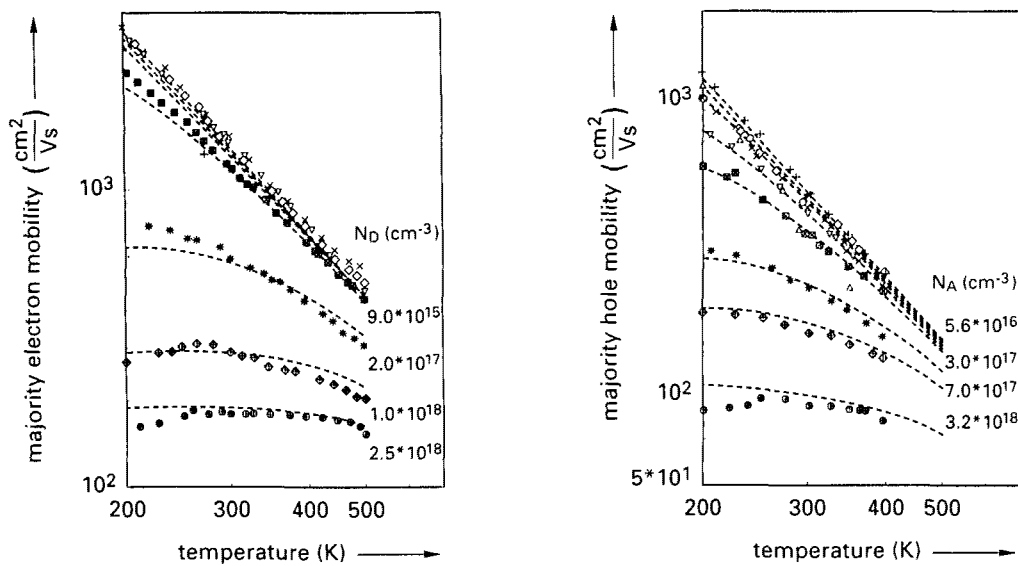
Figure 10 (left-hand side): Majority electron mobility as a function of temperature for various donor concentrations. Symbols represent experimental data [40, 41] and dashed lines represent model calculations.

Figure 11 (right-hand side): Majority hole mobility as a function of temperature for various acceptor concentrations. Symbols represent experimental data [42, 43] and lines represent model calculations.

3.8.5 Minority carrier diffusion length as a function of temperature

No direct experimental data on the minority carrier mobility as a function of temperature are available. In all published experiments [24, 44, 45] , only the minority carrier diffusion lengths (L) were measured as a function of temperature ($L = \sqrt{k\,T\mu\,\tau\,/\,q}$). The minority carrier lifetime (τ) was only measured at room temperature, while for its temperature dependence several *models* were used. Consequently the "experimental" results obtained for the minority carrier mobility as a function of temperature depend heavily on the temperature dependence used for the lifetime. It should be noted that these "experimental" minority carrier mobilities show a sharp increase with concentration at low temperatures [24, 44, 45] .

As already mentioned in Subsect. 2.1 limited experimental data is available on the carrier lifetime as a function of temperature. Consequently in the comparison between the *measured*
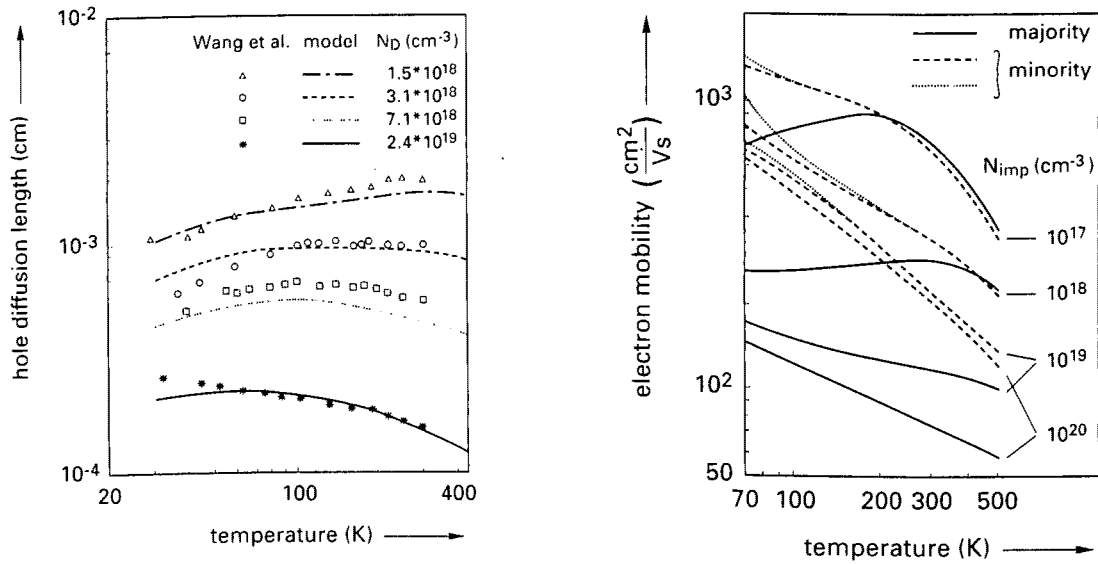
Figure 12 (left-hand side): Minority hole diffusion length as a function of temperature for various donor concentrations. Symbols indicate experimental data [45] and lines indicate model calculations.

Figure 13 (right-hand side): Calculated electron mobility as a function of temperature for various impurity concentrations: dashed lines indicate the minority electron mobility using complete ionization; dotted lines indicate the minority electron mobility using a temperature-dependent ionization (see Subsect. 3.10 and Fig. 16); and solid lines indicate the majority electron mobility.

minority hole diffusion length as a function of temperature and model calculations (see Fig. 12), also a model for the lifetime has to be used, which will be discussed in the next subsection. It should be noted that the mobility model described above contains no additional parameters to describe the temperature dependence of the minority carrier mobility. It is therefore interesting to note that the model calculations do not show the sharp increase with concentration at low temperatures mentioned above (see Fig. 13).

3.9 Temperature dependence of minority carrier lifetime

The minority carrier lifetime is determined by Shockley-Read-Hall and Auger recombination, which each may have their own temperature dependence. Consequently this lifetime is modelled as

$$\tau_e^{-1} = \left(\tau_{o,e}^{-1} + C_{SRH,e}\, N_A\right)\left(\frac{300}{T}\right)^\gamma + \left(C_{Aug,e}\, p^2\right)\left(\frac{T}{300}\right)^\delta. \tag{18}$$

Parameters in this expression were determined comparing data on the lifetime as a function of concentration (see Fig. 14) and data on the diffusion length as a function of temperature
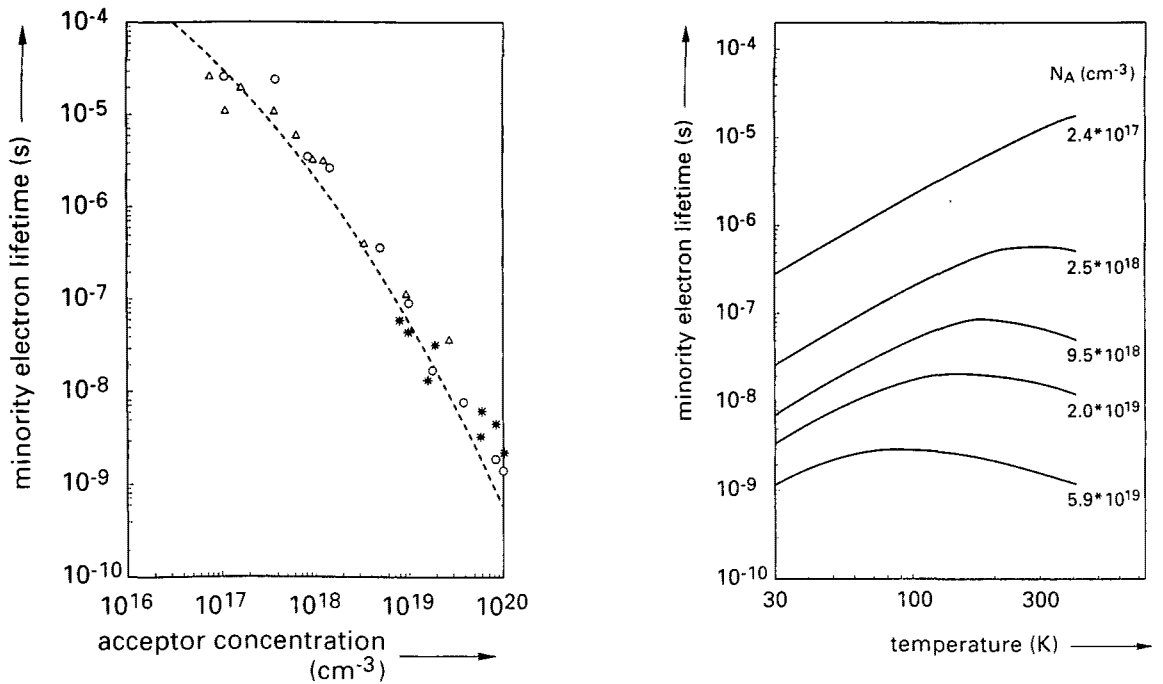
Figure 14 (left-hand side): Minority electron lifetime as a function of acceptor concentration at 300K. Symbols represent experimental data: asterisks [6]; triangles [19]; circles [20]. The dashed line represent a calculation using Eq. (18).

Figure 15 (right-hand side): Minority electron lifetime calculated as a function of temperature for various acceptor concentrations.

(for various concentrations; see Fig. 12) with model calculations. The values obtained are in agreement with the available experimental [20] and theoretical [46] information.

The minority electron lifetime as a function of temperature is shown in Fig. 15 for various acceptor concentrations. This temperature dependence is distinctly different from the dependences used in other publications: Swirhun [24] used one power dependence over the whole temperature range; Swirhun et al. [44] used a lifetime independent of temperature; and Wang et al. [45] used a lifetime linearly increasing with decreasing temperature.

3.10 Incomplete ionization

At low temperatures the impurity atoms are only partly ionized. The fraction of ionized impurity atoms can be calculated using a quite simple method (see e.g. page 12 of [17]). A problem of this method is that at a concentration of about 3×10^{18} cm^{-3} the ionization energy goes to zero. At that concentration the ionization is still incomplete, while the method cannot be used for higher concentrations. Kuzmicz published an analytical approximation for the ionized fraction as a function of temperature [47]. His results are based on a more sophisticated method and show complete ionization at high concentrations. Consequently, they can
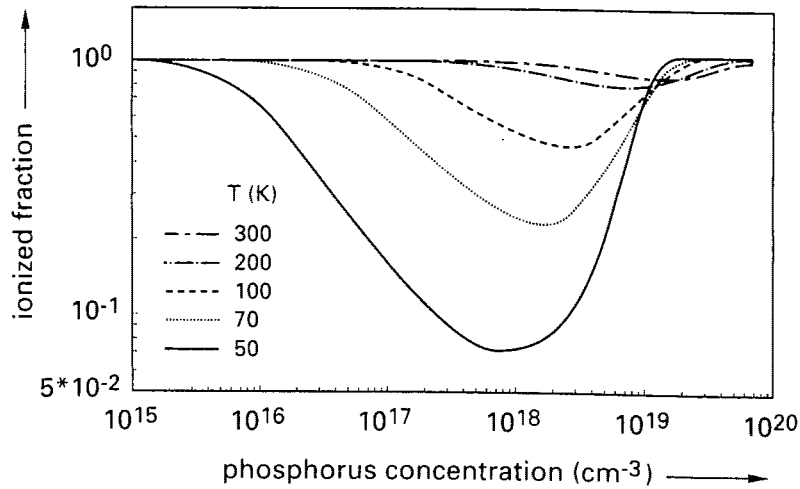
Figure 16: Ionized fraction as function of temperature for various dopant concentrations.

be used over the whole concentration range, but only for temperatures higher than 250 K. The ionized fraction shown in Fig. 16 is obtained with the former method allowing for negative activation energies.

Using this ionized fraction as a function of temperature and concentration, the influence of the incomplete ionization on the minority carrier mobility as a function of temperature is shown in Fig. 13. As can be seen from this figure, incomplete ionization has only a very small effect on the minority carrier mobility.

4 Intrinsic carrier concentration and bandgap narrowing

4.1 Intrinsic carrier concentration

The intrinsic carrier concentration, $n_{i,o}$, can be described by

$$n_{i,o}^2 = C T^3 e^{-q V_g / kT} ,$$ (19)

where V_g is the temperature dependent bandgap of intrinsic silicon [48]

$$V_g = 1.1700 - \frac{4.73 \times 10^{-4} T^2}{T + 636} \quad [V] .$$ (20)

Tuning the intrinsic carrier concentration to the data of Putley and Mitchell [49] yields $C = 3.97 \times 10^{31} cm^{-6} K^{-3}$.

Linearizing the expression for the temperature dependent bandgap implies that in Eq. (19) V_g has to be replaced by the *extrapolated* bandgap at $0K$, $V_{go} = 1.206 V$, and that for C the value $9.61 \times 10^{31} cm^{-6} K^{-3}$ should be used [49] .

38

4.2 Bandgap narrowing

The bandgap decreases at high doping concentrations, leading to an increase in effective intrinsic carrier concentration, $n_{i,e}$,

$$n_{i,e}^2 = n_{i,o}^2 \, e^{\, q \Delta V_{go} / kT} , \tag{21}$$

where ΔV_{go} depends on the dopant concentration, but is independent of temperature between $250K$ and $400K$ [50]. For ΔV_{go} the following empirical relation holds

$$\Delta V_{go} = V_{ref} \left\{ \ln \frac{N}{N_{ref}} + \sqrt{(\ln \frac{N}{N_{ref}})^2 + c} \right\} , \tag{22}$$
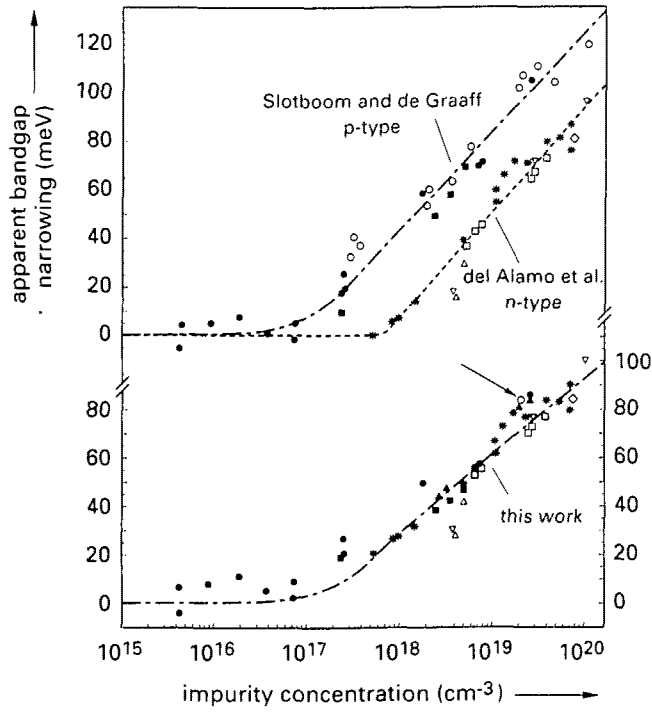
Figure 17: Apparent bandgap narrowing as a function of dopant concentration. In the upper part symbols represent data as reported in literature: p-type: open circles [6], solid circles [11], and solid squares [51]; n-type: asterisks [7, 12, 13], open upwards-directed triangles [37], open squares [52], open downwards-directed triangles [53], and diamonds [54]. The chain-dashed dashed curve represents the fit of [11], and the dashed curve represents the fit of [7, 13]. In the lower part solid upwards-directed triangles represent the data of [55] for p-type silicon and the other symbols represent the corrected values (see text). The chain-dashed curve respresents the new fit.

with for p-type: $V_{ref} = 9\,mV$; $N_{ref} = 1 \times 10^{17}\,cm^{-3}$; $c = 0.5$ [11]; and for n-type: $V_{ref} = 9.35\,mV$; $N_{ref} = 7 \times 10^{17}\,cm^{-3}$; $c = 0$ [7, 13] (see Fig. 17).

4.3 Unified bandgap narrowing

In most device experiments on bandgap narrowing the product $\mu\,n_{i,e}^{2}$ is actually determined. Consequently the values obtained for the bandgap narrowing are dependent on the value used for C in Eq. (19) and on the minority carrier mobility. Slotboom and de Graaff [11] used the majority electron mobility; Swirhun et al. [6] and del Alamo et al. [7, 12, 13] used the minority carrier mobilities indicated in Figs. 7 and 8. Moreover, all authors used different values for the parameter C.

We corrected all data in Fig. 17 using the value of C mentioned above and using the new mobility model (see Figs. 7 and 8). In contrast with the uncorrected data, the corrected data show no difference in bandgap narrowing for n- and p-type silicon and can be described by Eq. (22) (see Fig. 17). Recently a somewhat smaller value for C has been suggested [56]. Use of this value would imply an increase with about 5 meV for all corrected data on both n- and p-type silicon.
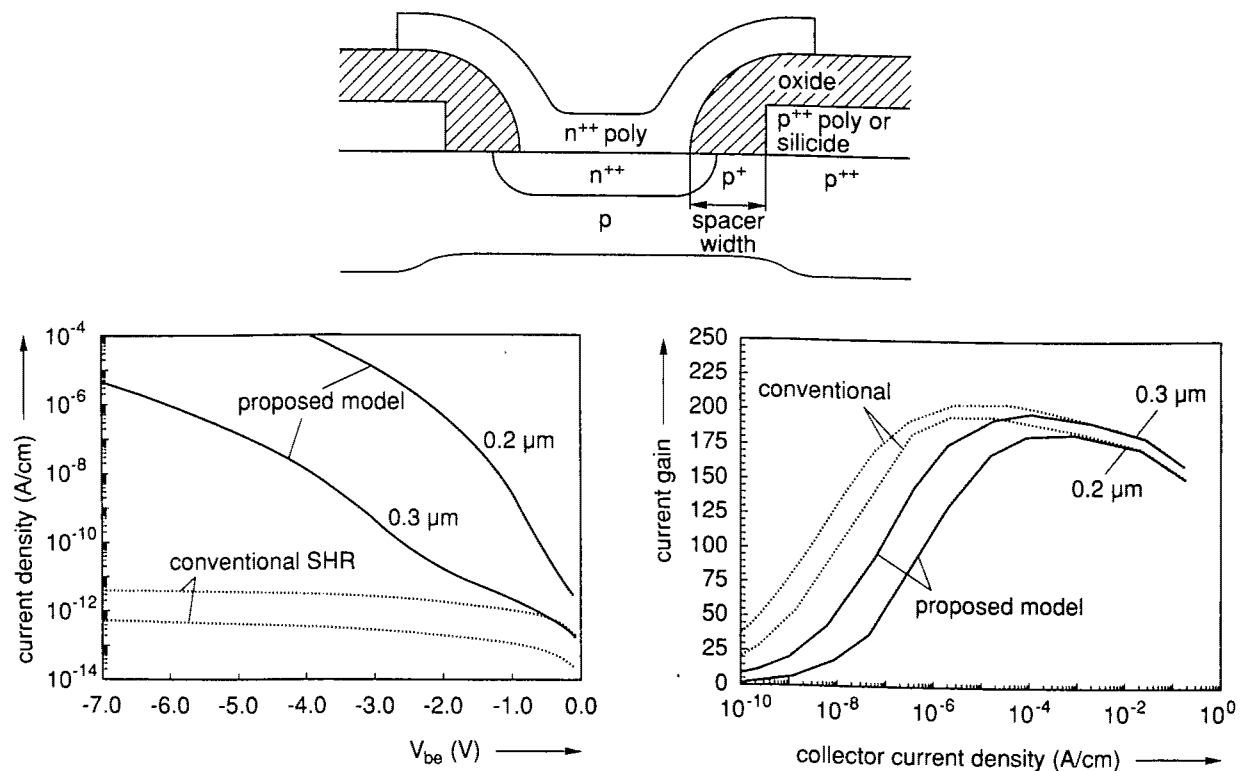
Figure 18: Results of a 2-D simulation of a double-poly structure with varying spacer width. The tunnelling effects in the generation/recombination model are clearly visible on the reverse characteristic (left-hand side) and current gain (right-hand side).

5 Conclusion

In the foregoing we have discussed recent developments in physical models for device simulation. The discussion was focussed on the incorporation of tunnelling effects in the generation-recombination of charge carriers, on the unified modelling of the majority and minority carrier mobility and on a resulting model for the bandgap narrowing valid for both n- and p-type silicon.

An important conclusion is that models for minority carrier mobility, intrinsic carrier concentration and bandgap narrowing should not be exchanged independently. They should be carefully tuned to each other and, most importantly, to all experimental data on these physical phenomena.

As conclusion to this survey two examples of device simulations using these new models are presented. In Fig. 18 a double-poly bipolar transistor is shown. A smaller oxide spacer results in a smaller lateral distance between the emitter and the base connection. Consequently the emitter-base junction at the side-wall will be steeper and the tunnelling contributions to both reverse leakage current and non-ideal base current increase. In Fig. 19 the current gain and cut-off frequency are shown of a standard transistor as obtained in a 1-D simulation. Starting with conventional models, subsequently the model for charge carrier mobility, bandgap narrowing and lifetime are replaced by the new models. From this figure it is clearly visible that the new models have a distinct, but partly *compensating* effect on the characteristics. This implies that the validity of a specific physical model for device simulation can hardly be proven by comparing simulated characteristics with measurements on standard transistors. Only sophisticated measurements on special test structures yield information that can be used to test a particular model unambiguously.
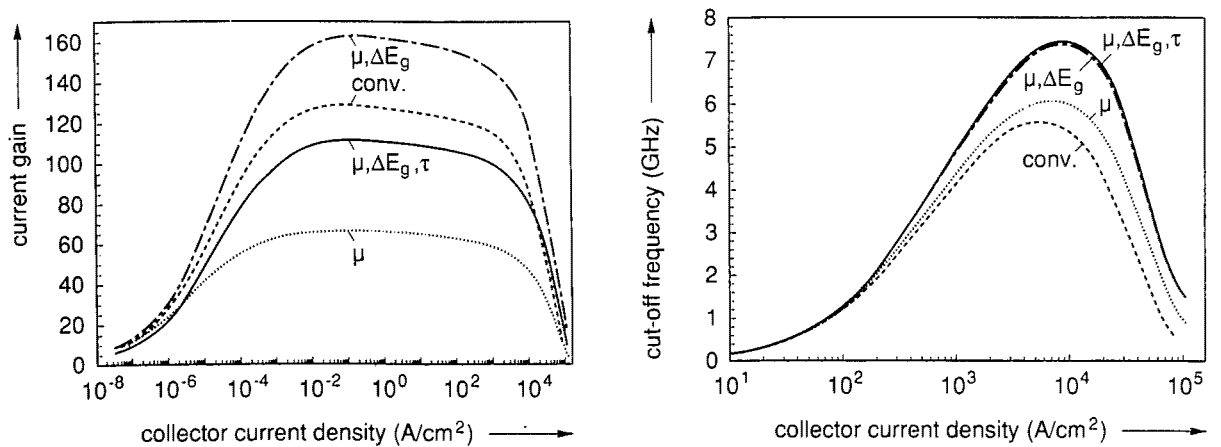
Figure 19: Current gain (left-hand side) and cut-off frequency (right-hand side) as function of the collector current obtained from a 1-D simulation using the various models discussed. Dashed line: conventional models; dotted line: new mobility model; dash-dotted line: new mobility and bandgap narrowing model; and solid line: new mobility, bandgap narrowing and lifetime model.

References

[1] J. del Alamo and R.M. Swanson, Forward-bias tunnelling current limits in scaled bipolar devices, Proc. SSDM, p. 283, 1986.

[2] J. del Alamo and R.M. Swanson, Forward-bias tunnelling: a limitatiion to bipolar device scaling, IEEE Electron Dev. Lett., 7 (1986) 629.

[3] J.C.S. Woo, J.D. Plummer and J.M.C. Stork, Non-ideal base current in bipolar transistors at low temperatures, IEEE Trans. Electron Dev., 34 (1987) 130.

[4] G.A.M. Hurkx, F.G. O'Hara and M.P.G. Knuvers, Modelling forward-biased tunnelling, Proc. ESSDERC'89, p. 793, 1989.

[5] G.A.M. Hurkx, D.B.M. Klaassen, M.P.G. Knuvers and F.G. O'Hara, A new recombination model describing heavy-doping effects and low-temperature behaviour, IEDM89 Techn. Digest, p. 307, 1989.

[6] S.E. Swirhun, Y.-H. Kwark and R.M. Swanson, Measurement of electron lifetime, electron mobility and bandgap narrowing in heavily doped p-type silicon, IEDM86 Techn. Digest, p. 24, 1986.

[7] J. del Alamo, S. Swirhun and R.M. Swanson, Simultaneous measurement of hole lifetime, hole mobility and bandgap narrowing in heavily doped n-type silicon, IEDM85 Techn. Digest, p. 290, 1985.

[8] S.E. Swirhun, J.A. del Alamo and R.M. Swanson, Measurement of hole mobility in heavily doped n-type silicon, IEEE Electron Dev. Lett., 7 (1986) 168.

[9] C.H. Wang, K. Misiakos and A. Neugroschel, Minority-carrier transport parameters in n-type silicon, IEEE Trans. Electron Dev., 37 (1990) 1314.

[10] C.H. Wang and A. Neugroschel, Minority-carrier transport parameters in degenerate n-type silicon, IEEE Electron Dev. Lett., 11 (1990) 576.

[11] J.W. Slotboom and H.C. de Graaff, Measurements of bandgap narrowing in Si bipolar transistors, Solid-State Electron., 19 (1976) 857.

[12] J. del Alamo, S. Swirhun and R.M. Swanson, Measuring and modeling minority carrier transport in heavily doped silicon, Solid-State Electron., 28 (1985) 47.

[13] J. del Alamo and R.M. Swanson, Measurement of steady-state minority carrier transport parameters in heavily doped n-type silicon, IEEE Trans. Electron Dev., 34 (1987) 1580.

[14] T. Kamins, Polycrystalline Silicon for Integrated Circuit Applications, Kluwer Academic Publishers, Boston, 1988.

[15] A.K. Kapoor and D.J. Roulston (Eds.), Polysilicon Emitter Bipolar Transistors, IEEE Press, New York, 1989.

[16] S. Selberherr, Analysis and Simulation of Semiconductor Devices, Springer, New York, 1984.

[17] H.C. de Graaff and F.M. Klaassen, Compact Transistor Modelling for Circuit Design, Springer, New York, 1990.

[18] W. Shockley and W.T. Read, Statistics of the recombinations of holes and electrons, Phys. Rev., 87 (1952) 835.

[19] J.D. Beck and R. Conradt, Auger-Rekombination in Si, Solid State Commun., 13 (1973) 93.

42

[20] J. Dziewior and W. Schmid, Auger coefficients for highly doped and highly excited silicon, Appl. Phys. Lett., 31 (1977) 346.

[21] A.G. Chynoweth, Ionization rates for electrons and holes in silicon, Phys. Rev., 109 (1958) 1537.

[22] G.A. Baraff, Distribution function and ionization rates for hot electrons in semiconductors, Phys. Rev., 128 (1962) 2507.

[23] R.J. van Overstraeten and H.J. de Man, Measurement of the ionization rates in diffused silicon p-n junctions, Solid-State Electron., 13 (1970) 583.

[24] S.E. Swirhun, Characterization of majority and minority carrier transport in heavily doped silicon, Ph. D. Dissertation, Stanford University, 1987.

[25] G. Vincent, A. Chantre and D. Bois, Electric field effect on the thermal emission of traps in semiconductor junctions, J. Appl. Phys., 50 (1979) 5484.

[26] G.A.M. Hurkx, On the modelling of tunnelling currents in reverse-biased p-n junctions, Solid-State Electron., 32 (1989) 665.

[27] E.O. Kane, Theory of tunnelling, J. Appl. Phys., 32 (1961) 83.

[28] S.H. Voldman, J.B. Johnson, T.D. Linton and S.L. Titcomb, Unified generation model with donar and acceptor-type trap states for heavily doped silicon, IEDM90 Techn. Digest, p. 349, 1990.

[29] N. Shigyo, H. Tanimoto, M. Norishima and S. Yasuda, Minority carrier mobility model for device simulation. Solid-State Electron., 33 (1990) 727.

[30] G. Masetti, M. Severi and S. Solmi, Modeling of carrier mobility against carrier concentration in arsenic-, phosphorus-, and boron-doped silicon, IEEE Trans. Electron Dev., 30 (1983) 764.

[31] D.B.M. Klaassen, A unified mobility model for device simulation, IEDM90 Techn. Digest, p. 357, 1990.

[32] B.K. Ridley, Quantum Processes in Semiconductors, Clarendon Press, Oxford, 1988.

[33] F.J. Blatt, Scattering of carriers by ionized impurities in semiconductors, J. Phys. Chem. Solids, 1 (1957) 262.

[34] J. Dziewior and D. Silber, Minority-carrier diffusion coefficients in highly doped silicon, Appl. Phys. Lett., 35 (1979) 170.

[35] D.D. Tang, F.F. Fang, M. Scheuermann, T.C. Chen and G. Sai-Halasz, Minority carrier transport in silicon, IEDM86 Techn. Digest, p. 20, 1986.

[36] D.E. Burk and V. de la Torre, An empirical fit to minority hole mobilities, IEEE Electron Dev. Lett., 5 (1984) 231.

[37] R.P. Mertens, J.L. van Meerbergen, J.F. de Nijs and R.J. van Overstraeten, Measurement of the minority-carrier transport parameters in heavily doped silicon, IEEE Trans. Electron Dev., 27 (1980) 949.

[38] F. Dannhäser, Die Abhängigkeit der Trägerbeweglichkeit in Silizium von der Konzentration der freien Ladungsträger - I, Solid-State Electron., 15 (1972) 1371.

[39] J. Krausse, Die Abhängigkeit der Trägerbeweglichkeit in Silizium von der Konzentration der freien Ladungsträger - II, Solid-State Electron., 15 (1972) 1377.

[40] S.S. Li and W.R. Thurber, The dopant density and temperature dependence of electron mobility and resistivity in n-type silicon, Solid-State Electron., 20 (1977) 609.

[41] S.S. Li, Semiconductor measurement technology, Nat. Bur. Stand., Special Publication 400-33, Washington DC, USA, 1977.

[42] S.S. Li, The dopant density and temperature dependence of hole mobility and resistivity in boron-doped silicon, Solid-State Electron., 21 (1978) 1109.

[43] S.S. Li, Semiconductor measurement technology, Nat. Bur. Stand., Special Publication 400-47, Washington DC, USA, 1979.

[44] S.E. Swirhun, D.E. Kane and R.M. Swanson, Temperature dependence of minority electron mobility and bandgap narrowing in p$^+$ Si, IEDM88 Techn. Digest, p. 298, 1988.

[45] C.H. Wang, K. Misiakos and A. Neugroschel, Temperature dependence of minority hole mobility in heavily doped silicon, Appl. Phys. Lett., 57 (1990) 159.

[46] D.B. Laks, G.F. Neumark, A. Hangleiter and S.T. Pantelides, Theory of interband Auger recombination in n-type silicon, Phys. Rev. Lett., 61 (1988) 1229.

[47] W. Kuzmicz, Ionization of impurities in silicon, Solid-State Electron., 29 (1986) 1223.

[48] C.D. Thurmond, The standard thermodynamic functions for the formation of electrons and holes in Ge, Si, GaAs and GaP, J. Electrochem. Soc., 122 (1975) 1133.

[49] E.H. Putley and W.H. Mitchell, The electrical conductivity and Hall effect of silicon, Proc. Phys. Soc. London, A72 (1958) 193.

[50] J.W. Slotboom, The pn-product in silicon, Solid-State Electron., 20 (1977) 279.

[51] M.Y. Ghannam, Contribution to the study and reduction of the base current of silicon bipolar transistors, Ph. D. Dissertation, Katholieke Universiteit Leuven, 1985.

[52] A.W. Wieder, Emitter effects in shallow bipolar devices: Measurements and consequences, IEEE Trans. Electron Dev., 27 (1980) 1402.

[53] A. Neugroschel, S.C. Pao and F.A. Lindholm, A method for determining energy bandgap narrowing in highly doped semiconductors, IEEE Trans. Electron Dev., 29 (1982) 894.

[54] G.E. Possin, M.S. Adler and B.J. Baliga, Measurements of the p-n product in heavily doped epitaxial emitters, IEEE Trans. Electron Dev., 31 (1984) 3.

[55] R.R. King, Studies of oxide-passivated emitters in silicon and applications to solar cells, Ph. D. Dissertation, Stanford University, 1990.

[56] M.A. Green, Intrinsic concentration, effective densities of states and effective mass in silicon, J. Appl. Phys., 67 (1990) 2944.